Temporally-Resolved, Infrared Spectra from the Detonation of Advanced Munitions

Joe Motos Gordon, Kevin C. Gross*, Glen P. Perram
Air Force Institute of Technology, Dept. of Engineering Physics, Wright-Patterson AFB, OH 45433

ABSTRACT

A suite of instruments including a 100 kHz 4-channel radiometer, a rapid scanning Fourier-transform infrared spectrometer, and two high-speed visible imagers was used to observe the detonation of several novel insensitive munitions being developed by the Air Force Research Laboratory. The spectral signatures exhibited from several different explosive compositions are discernable and may be exploited for event classification. The spectra are initially optically thick, resembling a Planckian distribution. In time, selective emission in the wings of atmospheric absorption bands becomes apparent, and the timescale and degree to which this occurs is correlated with aluminum content in the explosive formulation. By analyzing the high-speed imagery in conjunction with the time-resolved spectral measurements, it may be possible to interpret these results in terms of soot production and oxidation rates. These variables allow for an investigation into the chemical kinetics of explosions and perhaps reveal other phenomenology not yet readily apparent. With an increased phenomenological understanding, a model could be created to explain the kinetic behavior of the temperature and by-product concentration profiles and thus improve the ability of military sensing platforms to identify explosive types and sources.

Keywords: High explosive, detonation, RDX, aluminum, combustion, fireball, spectroscopy, FTS, classification

1. INTRODUCTION

The ability to quickly identify and classify an explosive type and employ theater assets to further survey or neutralize its source is of great concern for battlefield commanders. A key to the identification and classification steps is a robust sensing platform able to efficiently characterize detonation signatures. An important prerequisite is the understanding of event phenomenology so that a effective, small, low-power sensor can be developed. For this purpose, our research group has fielded rapid-scan Foruier-transform spectrometers, radiometers, and high-speed imagers to various test ranges to remotely collect post-detonation combustion (PDC) signatures from detonations of various $C_vH_wN_xO_yAl_z$-based high-explosives (HEs). To date, the focus has been on interpreting the spectral signatures for the purpose of understanding event phenomenology. A significant outcome was the development of a low-dimensional physics-based model that was capable of describing with high fidelity the observed spectra in terms of a temperature, size, and handful of by-product concentrations (primarily H_2O, CO_2, and soot). The model affords significant reduction in the spectral dimensionality with ~500–2000 points being replaced by 5–7 parameters. Using this model against time-resolved spectra (8 Hz at $\Delta\tilde{\nu} = 1.93$ cm^{-1}) collected in the BRILLIANT FLASH II field experiment, estimates of the hydrogen-to-carbon ratio R = H:C were made from the spectra of several high-explosives and were in agreement with the stoichiometry of the starting material. Additionally, the fireball cooling rate $\partial T/\partial t$ was highly correlated with the mass of the explosive. By reducing the dimensionality of the spectral datacube to a handful of "orthogonal features" (from an information content perspective), we demonstrated that high-explosive classification is possible with midwave infrared (MWIR) spectral signatures.

The various explosive classes examined during the BRILLIANT FLASH II test exhibited large differences in HE stoichiometry. Distinguishing different explosives with similar relative amounts of hydrogen and carbon will be more difficult, given that their PDC in the oxygen-rich atmosphere will tend to produce H_2O and CO_2 in similar relative quantities. However, upon detonation different explosives will proceed to final products through different reaction pathways, and the fireball's temporal signature may be sensitive to these differences, particularly at early times when the combustion processes are more representative of the initial conditions. In Fourier-transform spectroscopy (FTS), temporal and spectral resolution are approximately inversely related, and our previous PDC measurements have favored spectral resolution so that emitting species could be more easily identified. This has made it difficult to study the global kinetic processes at work in the fireball. By degrading the resolution of previous spectral measurements with post-processing, it was found

Further author information
* KCG: kevin.gross@afit.edu, +1 (937) 255-3636 x4558
GPP: glen.perram@afit.edu, +1 (937) 255-3636 x4504

Sensors and Systems for Space Applications III, edited by Joseph L. Cox, Pejmun Motaghedi
Proc. of SPIE Vol. 7330, 733006 · © 2009 SPIE · CCC code: 0277-786X/09/$18 · doi: 10.1117/12.818166

Table 1. Listing of some of the constituent materials and nominal quantities for the 22 test items.

EXPLOSIVE			LINER		TEST ITEM	INSTRUMENTATION	
HE Type	**HE RDX Content**	**HE Al Content**	**Liner Al Content**	**Liner Volume %**	**Final Test Item Al Content**	**FTS Resolution (Temporal / Spectral)**	**Phantom Camera Frame Rate (frames/s)**
A	Low	High	Low	w	None	82 Hz at 16 cm^{-1}	10,000
B	Medium	Low	Medium	x	Low	54 Hz at 8 cm^{-1}	
C	High	None	High	y	Medium		
				z	High		

that a four-times reduction in resolving power ($\Delta\tilde{\nu}$ = 7.71 cm^{-1}) had a minimal impact in the precision of temperature, size, and by-product concentrations derived from the model. Thus, improving temporal resolution by degrading resolving power could lead to improved understanding of the kinetic aspect of fireball phenomenology.

To begin studying the kinetic piece of the fireball problem in greater detail, measurements of fireballs arising from various HEs fashioned from aluminized RDX were recently made at a test range at Eglin Air Force Base. By using a faster interferometer operating at $\Delta\tilde{\nu}$ = 3.86 or 7.71 cm^{-1}, spectra were acquired at rates of 55 or 82 Hz. A four-channel, 100 kHz radiometer and two high-speed visible cameras provide band-integrated intensities and imagery to augment the FTS measurements. This paper presents an overview of the test and a summary of initial findings discovered in the early stages of this ongoing research effort.

2. EXPERIMENTAL

The Reactive Liner Naturally Fragmenting Test Unit (NFTU) field tests were developed to meet Department of Defense (DoD) Insensitive Munition (IM) requirements of General Purpose (GP) warheads. The IM requirement is part of an effort to improve fielding, storage, and safety of current inventory GP bombs by reducing their sensitivity to ship-board and munitions storage fires as well as sympathetic detonations. The tests were conducted over 15 April – 1 May 2008 at the Advanced Warhead Experimentation Facility (AWEF) of the Air Force Research Laboratory (AFRL) at Eglin Air

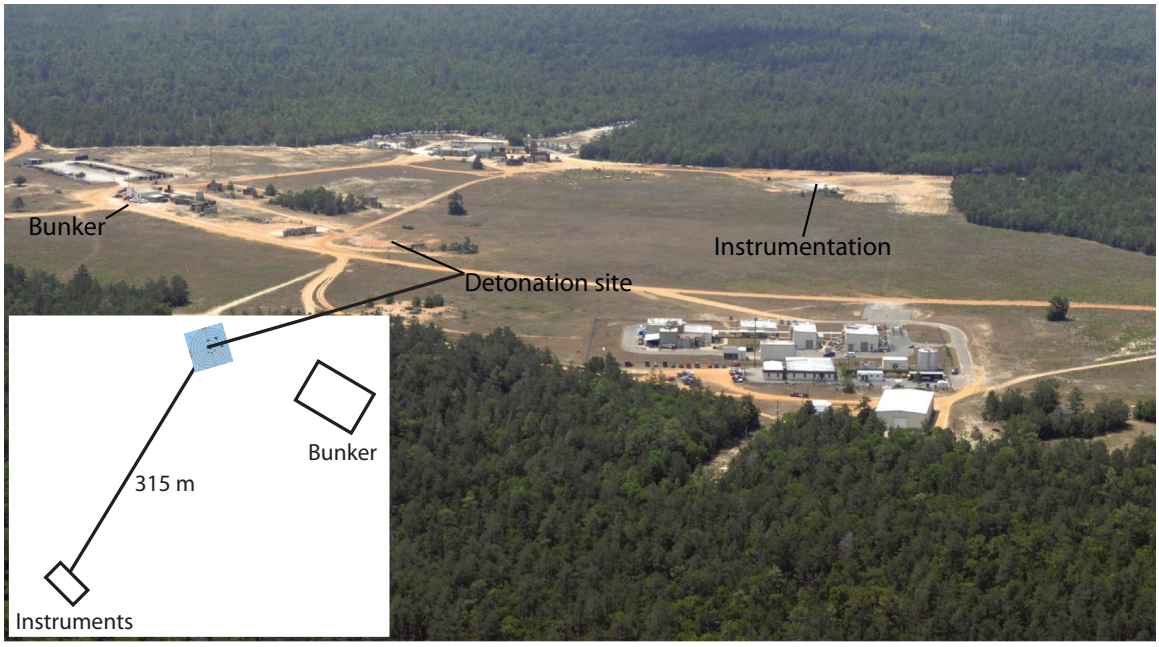

Fig. 1. Aerial view of the AWEF test range. The blast arena where the test items were detonated is highlighted by the concentric rings at the top of the inset schematic.

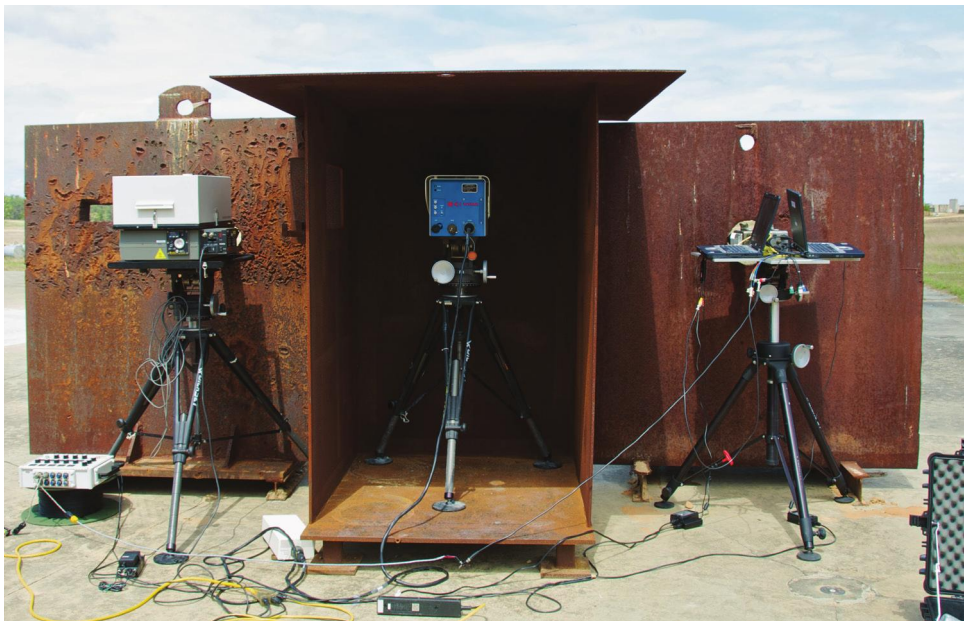

Fig. 2. Left to right, the ABB-Bomem MR-254 FTS, CI Systems ColoRad radiometer, and pair of Phantom 5.1 and 7.1 cameras. Each is peering through a hole from behind thick iron armor shielding. A plywood roof was subsequently installed to shield the instruments from heating via direct sunlight, thereby minimizing the effects of self-emission in the InSb channel of the FTS and the InSb and HgCdTe channels of the radiometer.

Force Base, Florida. A factorial Design-of-Experiments was conducted by AFRL engineers to examine the main effects and interactions of the various liner and explosive types. Thirteen optical signatures were successfully collected out of 22 scheduled detonations. These detonations were comprised of three distinct types of liners and three distinct types of explosives and their various combinations. Table 1 summarizes some important test parameters. The liners were melt-cast thermoplastic materials with aluminum content varying from low to high and arranged along the inside walls of a warhead. The explosives were RDX-based (cyclotrimethylene-trinitramine, $C_3H_6N_6O_6$) melt-cast formulations also with varying aluminum content from none to high.

The following is a brief overview of the reactive liner NFTU tests. Figure 1 provides a birds-eye view of the test range. The instrument suite was placed on a stable concrete pad approximately 315 m from the center of the blast arena and was the only location at the AWEF that had a direct, unobstructed line-of-sight to the target at a safe standoff distance. All equipment was remotely triggered from within the hardened command and control center. Time-resolved infrared spectra were collected using an ABB-Bomem MR-254 FTS operated at 82 Hz with a nominal spectral resolution of 16 cm^{-1} ($\Delta\tilde{\nu}$ = 7.71 cm^{-1}) using InSb (1800–10,000 cm^{-1}) and InGaAs (5600–10,000 cm^{-1}) detectors. A few events were collected at 8 cm^{-1} (3.86 cm^{-1}) resolution at a rate of 55 Hz. The interferograms were over-sampled at half-HeNe wavelengths putting the Nyquist frequency at 15,802 cm^{-1} which is well beyond the response of the InSb and InGaAs detectors. The interferometer was fitted with 76 mrad optics providing a 24 m diameter field-of-view (FOV) at the target. Bore-sighted video indicated that the fireballs consistently under-filled the FOV. Figure 2 shows additional instruments that were deployed to record other aspects of the incoming optical signatures. A CI Systems Colorad four-channel radiometer using InSb, InGaAs, HgCdTe, and Si detectors, each with a distinct narrow optical density filter, collected broadband intensity spectra at 100 kHz. Phantom 5.1 and Phantom 7.1 high-speed digital video cameras operating between 2000–8000 fps were used to study fireball growth and characterize shockwave dynamics. A Canon XL-1 digital video camera served as a witness camera and the audio channel was used to measure the time for the pressure wave to reach the location of the equipment.

A low-temperature (10°C below ambient to 80°C) wide-area blackbody (BB) source and a high-temperature (1250°C) cavity blackbody source were used to calibrate the FTS detector several times each day. The calibration measurements were performed before and after each detonation optical signature were collected. The wide-area BB was placed within a few inches of the FTS entrance aperture and thus over-filling the FOV. Several low-temperature blackbody measure-

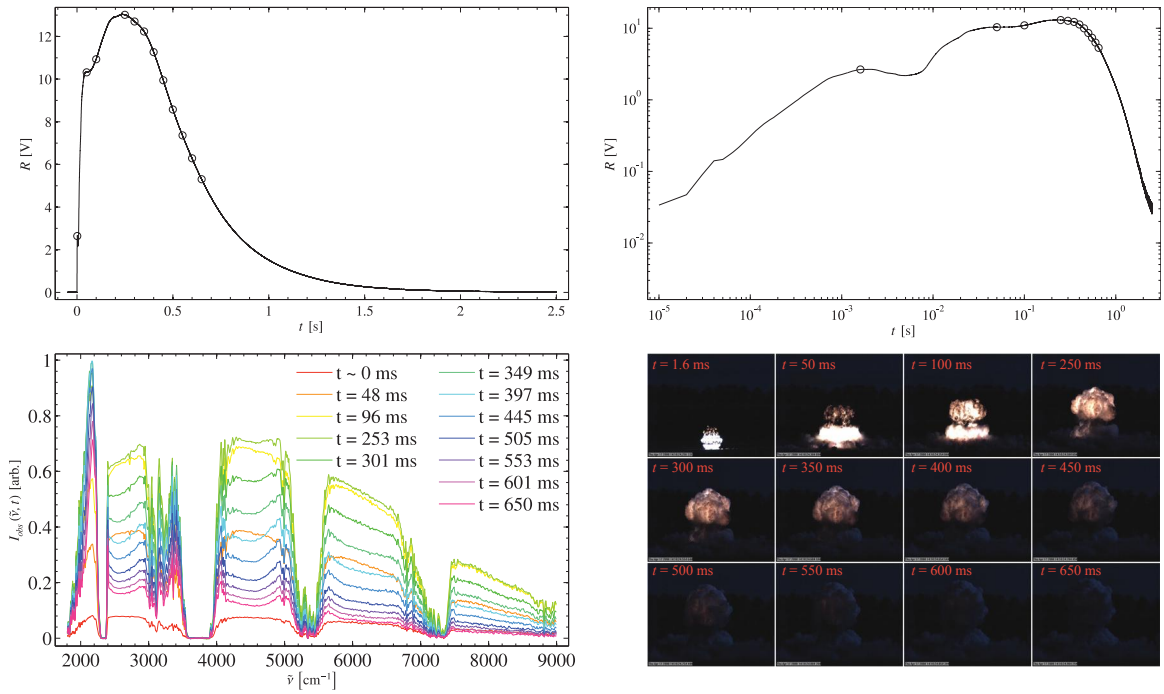

Fig. 3. Overview of the radiometric, spectro-radiometric, and high-speed imagery collected from an aluminized RDX fireball. *Top-left panel*: Band-integrated radiometric response of the InSb channel of the CI Systems ColoRad radiometer. *Top-right panel*: Same band-integrated radiometric profile shown on a log-log scale. Open circles indicated the times corresponding to the spectra and imagery shown in the bottom panels. *Bottom-left panel*: Time-evolution of the MWIR spectra captured by the ABB-Bomem MR-254 FTS. *Bottom-right panel*: Color imagery captured by the Phantom v7.1 camera. A majority of the pixels illuminated in the first frame were saturated.

ments were made, enabling an accurate determination of both detector response (gain) and instrument self-emission (offset) between 1750–3000 cm^{-1}. Instrument self emission was important between 1750–2500 cm^{-1}. A high-temperature cavity BB source (T~1200 K) was used to extend the detector response to 10,000 cm^{-1}. The path between the FTS and the cavity BB source was approximately 6 m. When calibrating against the cavity BB, the field stop of the FTS was minimized to cover an area only slightly larger than the BB source aperture in order to minimize the contribution of background radiation. The cavity BB was shielded from direct sunlight to minimize reflection of solar radiation off of the faceplate and promote a stable temperature. Given the precautions taken in the cavity BB measurements, it was reasonable to assume that the only source of photons beyond 3000 cm^{-1} was from the cavity, enabling a relative measure of the detector response (gain) via division by the appropriate Planckian distribution. In other words, both instrument self-emission and background radiation (i.e., radiation generated by or reflected from the warm faceplate of the BB) could be ignored above 3000 cm^{-1}. An absolute scale for the relative gain curve between 3000–10,000 cm^{-1} was established by comparison with the gain curve already determined via the wide-area source where they overlap near 3000 cm^{-1}.

3. ANALYSIS

Figure 3 presents an overview of the data collected by our primary suite of instruments for the detonation of an aluminized RDX explosive. The uncalibrated band-integrated response of the InSb channel on the CI-Systems radiometer are shown in the top two panels, and spectra and visible imagery at select times are provided in the bottom panel. In the MWIR, the duration of the event is approximately 2 s, and decays to e^{-3} of the peak response in ~1.25 s. The top-right panel provides the same information on a log-log plot so that the full dynamic range of both the temporal and intensity axes can be visualized. There are two distinct time scales, the first associated with the initial and rapid detonation (0–5 ms), and the second associated with the post-detonation combustion (5–1500 ms). The initial detonation is a combustion reaction occurring under extreme conditions, with stored oxygen serving as the oxidizing materials. The fireball rapidly expands, and near the end of the this initial detonation, the radiant emission in the MWIR begin to decrease (cooling by expansion). Visible imagery indicates that luminous emissions near the top of the fireball have substantially

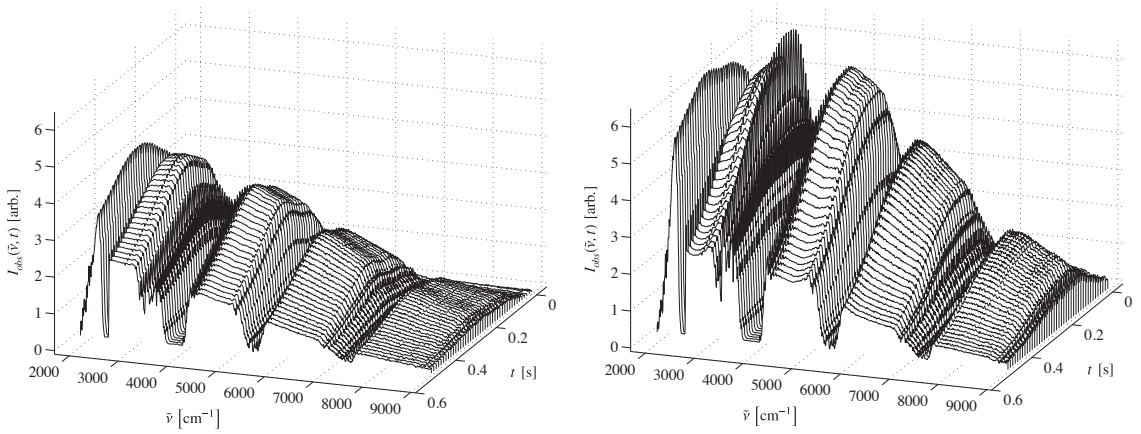

Fig. 4. Time-resolved spectral datacubes for the first 0.5 s of a low-Al (a) and high-Al (b) RDX detonation fireball. Effects of detector response (gain) have been accounted for and the scale for the ordinate axis is the same in both plots.

decreased, appearing dark and sooty. At the same time turbulent eddies can be seen forming. The primary shockwave then reflects off the ground and proceeds back through through the fireball causing shock heating and with it re-ignition of the non-luminous sooty regions and enhanced (brighter) combustion throughout. This post-detonation combustion process continues as atmospheric oxygen is brought into the fireball through turbulent mixing. Visible imagery indicates that the fireball reaches a peak area after about 200–300 ms and remains at about the same size, although the morphology changes and its center-of-mass increases in height with time. The complex interplay of fluid dynamics and combustion chemistry produce a fireball that is both highly luminous in some regions and a sooty black in others, resulting in an interesting temporal variation of the total, band-integrated intensity, particularly at early times. The band-integrated intensity reaches a maximum at approximately 250 ms, after which cooling by radiative emission and turbulent mixing with air cause the signal to decay back to ambient conditions within a few seconds.

At early times ($0 \leq t \leq 150$ ms), the spectra indicate an optically-thick fireball with continuum emission from soot masking out selective emission from gaseous by-products. At these times, the only strong spectral features are due to absorption by atmospheric water and carbon dioxide. Shortly after the peak total emission occurs (t~250 ms), moderate amounts of selective emission are observed in the wings of strong atmospheric absorption bands, likely due to radiant emission from hot H_2O (3200–4200, 5600–6000 cm^{-1}) and CO_2 (2200–2450, 4800–5200 cm^{-1}) within the fireball. As atmospheric oxygen is made available through turbulent mixing, the carbonaceous soot can be oxidized to CO and then to CO_2, leading to a less thick (i.e., slightly more transparent) fireball. Similar spectral features have been observed in TNT detonation fireballs and understood in terms of the simple phenomenological model briefly described in the introduction and discussed more thoroughly in the references.[2-6] Preliminary results of fitting this spectral model to the data (not shown) have been fair, capturing the gross features of the spectral variation in the data. However, the fit residuals exhibit small, but non-negligible systematic errors, and improvements to the model are currently being investigated.

Two events, a low-Al and a high-Al RDX formulation, are now analyzed in greater detail. Figure 4 presents time-resolved spectral datacubes for the first 500 ms for each type. The radiant emissions from the high-Al formulation are brighter in the MWIR. Continuum radiation from soot dominates the spectral emissions from both fireballs. At later times, the high-Al RDX fireball begins to exhibit selective emission in the wings of the atmospheric absorption bands. To facilitate a comparison of the relative spectral features, normalized fireball spectra corresponding to both formulations are displayed in Figure 5 at an early (t~200 ms) and later (t~600 ms) time. At 200 ms, both spectra appear Planckian in nature. By 600 ms, the differences in the spectral features are pronounced. The low-Al formulation is still strongly dominated by continuum emission, whereas the high-Al fireball exhibits much stronger selective radiation. This may indicate a relationship between the aluminum content in the explosive mixture and soot production and oxidation processes in the fireball, since oxidation of soot is necessary to make the fireball optically thin enough to observe emissions from gaseous combustion by-products such as H_2O and CO_2.

Soot chemistry can be indirectly studied—in an approximate way—by examination of the continuum emission. This can be achieved by fitting a single-temperature Planckian intensity distribution to the regions spectra in which molecular line

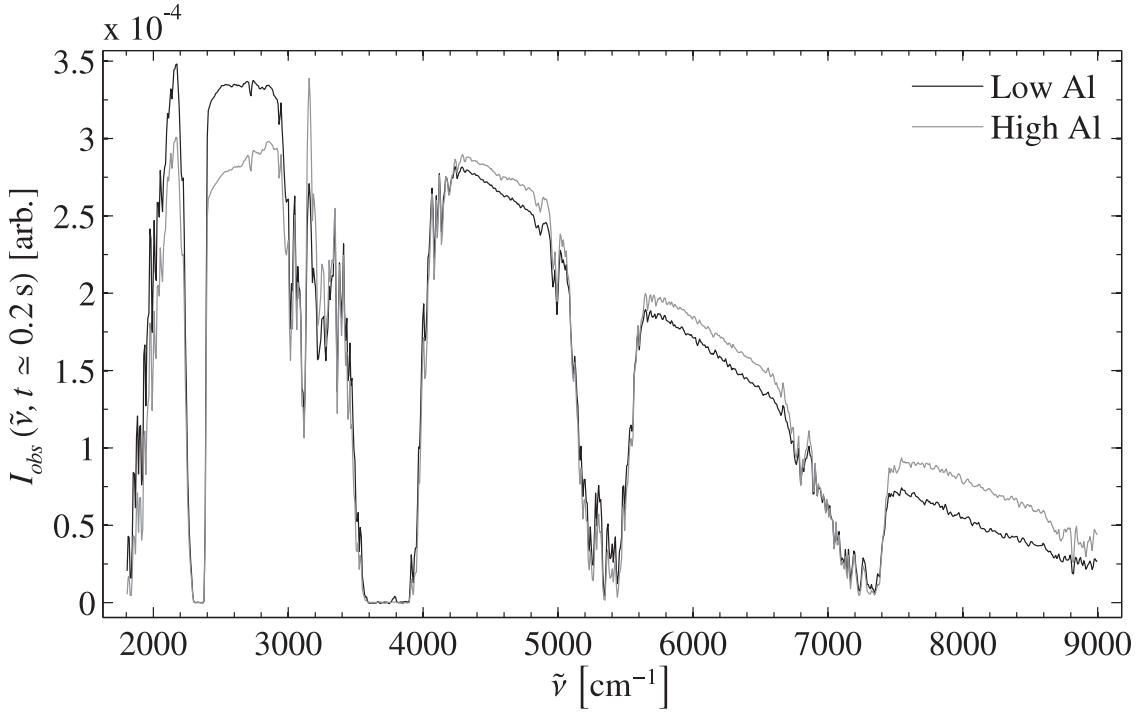

(a)

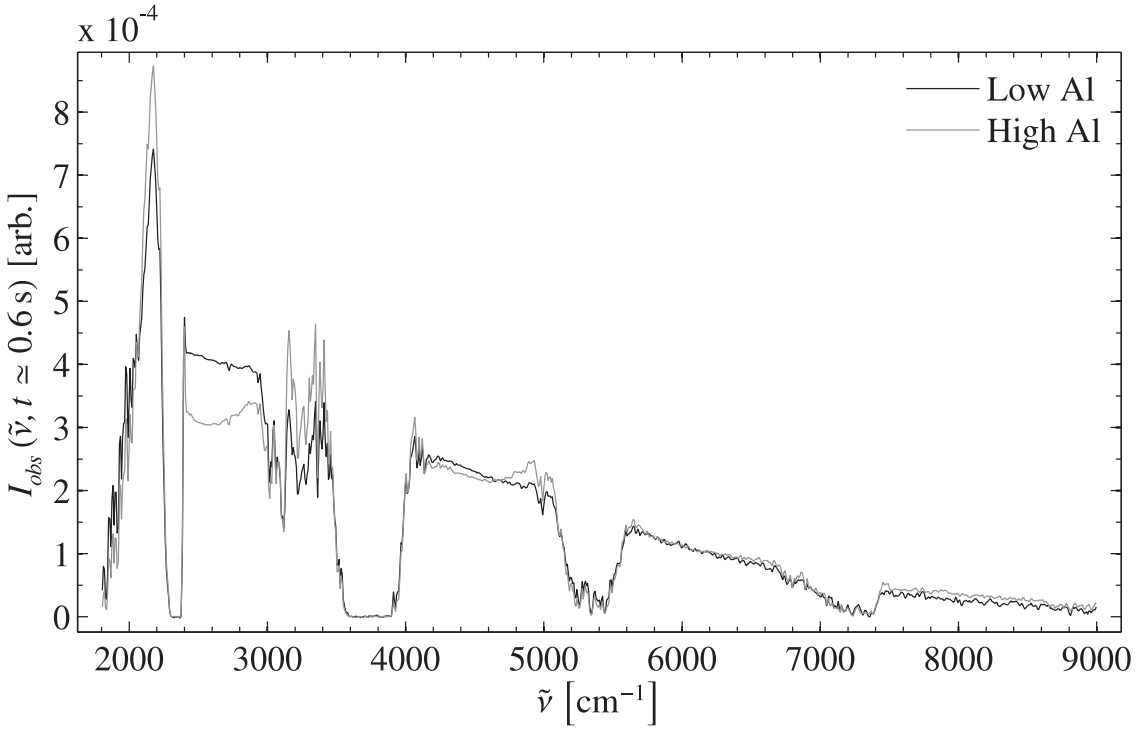

(b)

Fig. 5. Normalized spectra corresponding to RDX containing low (—) and high (—) aluminum content at (a) 0.2 s and at (b) 0.6 s. At early times, both spectra are dominated by continuum radiation from the soot. As time progresses, the high-Al RDX exhibits more selective emission near 2100, 3200, and 4950 cm^{-1}.

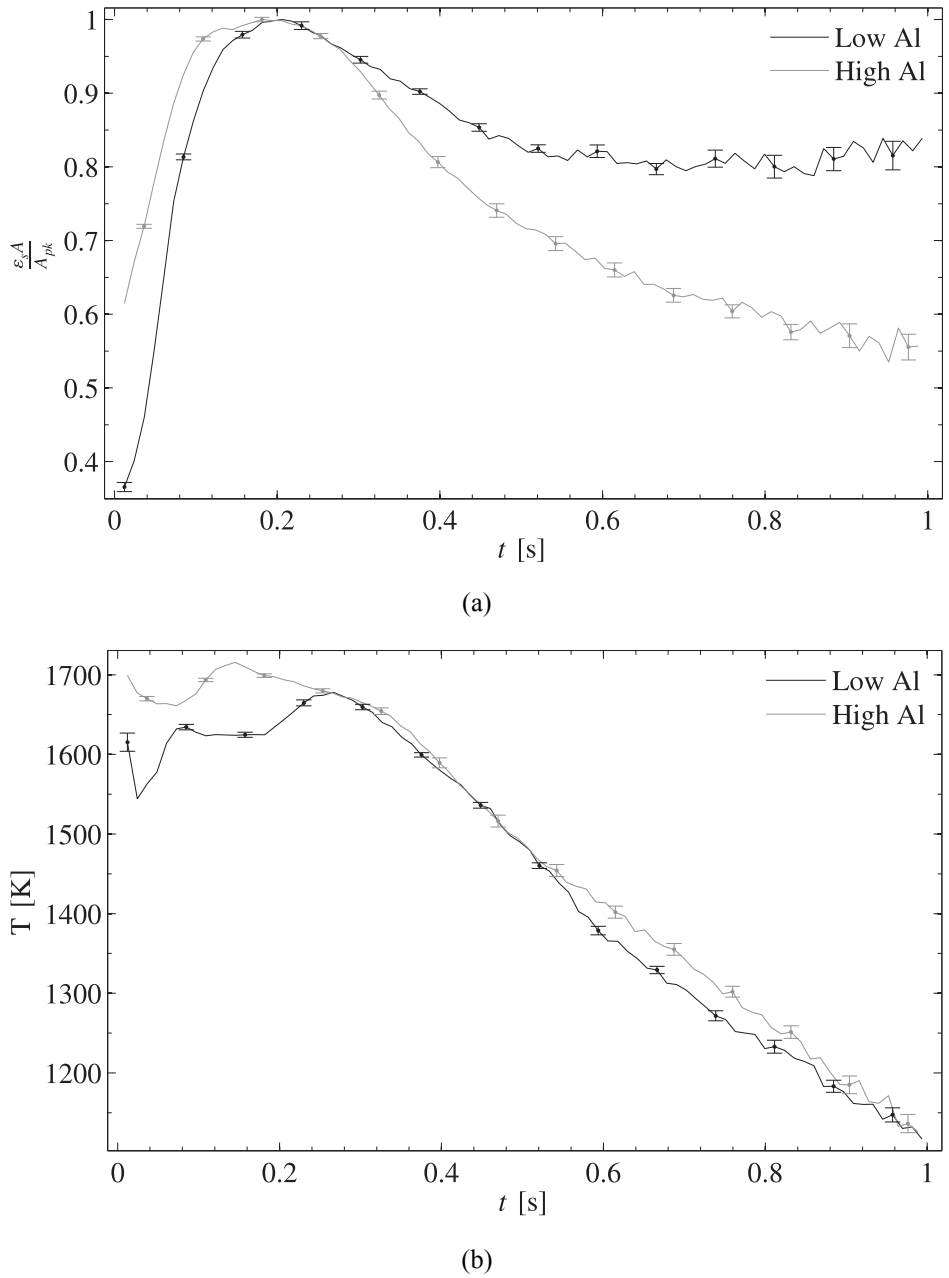

Fig. 6. (a) Peak-normalized emissivity-area and (b) temperature curves for the low-Al and high-Al RDX fireballs obtained by fitting a Planckian distribution to spectral regions free from selective emission (4400–4700 and 5800–6500 cm^{-1}).

emission is unimportant and continuum radiation from hot particulate matter dominates. To this end, the following model was used to make estimates of the temperature T and emissivity-area product $\varepsilon_s A$

$$I_{obs}(\tilde{\nu}, t) = \tau(\tilde{\nu})\, \varepsilon_s A(t)\, B(\tilde{\nu}, \mathrm{T}(t)) \tag{1}$$

where τ accounts for atmospheric absorption and B is the Planckian distribution for radiance. The model was fit to the spectral regions 4400–4700 cm^{-1} and 5800–6500 cm^{-1} for times up to approximately 1 s. At longer times, the spectrum was too noisy to extract reliable fit parameters. Figure 6 presents the results of estimating T and $\varepsilon_s A$ from the time-

resolved spectra corresponding to both the low-Al and high-Al RDX formulations. Error bars are occasionally displayed so that the trending of fit uncertainty can be assessed. The $\varepsilon_s A$ curves are normalized by the peak area. We noted previously that the fireball reaches its maximum size around 200–300 ms, and this is approximately the same time at which MWIR emissions reach their peak total intensity (*cf*. Figure 3). Additionally, imagery also suggests sooty fireballs and the spectral emissions dominated by continuum radiation and absent of line emission corroborate this observation. Given this, an initial emissivity of one is assumed, and the initial rise in the normalized $\varepsilon_s A$ curve is due to the fireball's expansion. Imagery also suggests that the fireball area remains approximately constant (or continues to grows slightly), so that the subsequent decay in $\varepsilon_s A$ is likely due to a decrease in ε_s. At times after the peak, the normalized $\varepsilon_s A$ curves may reveal differences in the kinetics of soot production and oxidation in the low-Al and high-Al formulations. Two possible explanations for the larger decrease in $\varepsilon_s A$ for the high-Al formulation may be (1) that its soot oxidation rates are higher at later times or (2) that its soot production rates are lower at earlier times. Both possibilities (or a combination thereof) could lead to the high-Al formulation having a more optically thin fireball at later times. Note that the two explosive charges feature different aluminum content in both the explosive mixture and the reactive liner. To assess which (if any) variable is more influential in the observed results, it will be necessary to examine spectral data from formulations in which the aluminum content of the reactive liner and/or HE material is fixed. There are likely other possible explanations for the observed behavior (e.g., the differences observed are to within the natural variance of a large number of measurements), and at this point, nothing definitive can be stated regarding soot production and consumption mechanisms and rates. This is a challenging topic posing both theoretical difficulties and experimental challenges under ideal laboratory conditions.[7] Moving to the harsh and highly non-ideal environment of a detonation fireball exploded in an uncontrolled environment only exacerbates the problem. What is significant here is that proper interpretation of the time-resolved spectra will be highly valuable in the development of a simplified "zeroth-order" kinetic fireball model.

The temperature profiles for the low-Al and high-Al formulations are similar. Differences are more profound at earlier times, but are also significant between 600–900 ms. The high-Al formulation exhibits a higher temperature both early on and at later times, and this is not inconsistent with the additional heat release that would presumably accompany the enhanced soot oxidation possibly occurring at later times in this fireball.

4. CONCLUSIONS

A recent field experiment has resulted in the collection of a rich set of radiometric, spectro-radiometric, and high-speed imagery measurements of various aluminized RDX high explosive detonation fireballs. The improved temporal resolution of the spectral measurements will benefit the development of a highly-simplified global kinetic model for detonation fireballs. Variations in aluminum content substantially alter the fireball chemistry, and a proper interpretation of the time-resolved spectral emissions is key to understanding the kinetic behavior of the by-products. Combining imagery analysis with simple planckian fits to the spectral data indicate a possible correlation between the aluminum content in the high-explosive with soot production and oxidation rates.

REFERENCES

[1] Cooper, Paul W. Explosives Engineering. VCH Publishers, New York, New York, 1996.

[2] Gross, Kevin C. Phenomenological model for infrared emissions from high-explosive detonation fireballs. Ph.D. Dissertation, AFIT/DS/ENP/07-03, Air Force Institute of Technology, 2007.

[3] Gross, Kevin C., Joseph Wayman, Glen P. Perram, "Phenomenological fireball model for remote identification of high-explosives." Proceedings of the SPIE-The International Society of Optical Engineering, 2007, 6566, Automatic Target Recognition XVII, p. 656613

[4] Gross, K.C.; Perram, G.P.; Tuttle, R.F. "Modeling infrared spectral intensity data from bomb detonations." Proceedings of the SPIE-The International Society of Optical Engineering, 2005, 5811 (1), pp. 100-11.

[5] Orson, Jay A., William F. Bagby, Glen P. Perram, "Infrared signatures from bomb detonations." Infrared Physics & Technology, Apr 2003, 44 (2), p. 101, 7p.

[6] Gross, Kevin C. and Glenn P. Perram, "The phenomenology of high explosive fireballs from fielded spectroscopic and imaging sensors for event classification." International Journal of High Speed Electronics & Systems, Mar 2008, 18 (1), p.19-29, 11p.

[7] Modest, Michael F. *Radiative Heat Transfer*, McGraw-Hill, Inc. New York, New York, 1993.